Modal analysis on unstructured meshes of the dispersion properties of the $P_1^{NC} - P_1$ pair

P.-E. Bernard [a], J.-F. Remacle [a], V. Legat [a]

[a] *Institute of Mechanical, Materials and Civil Engineering, Université catholique de Louvain, Avenue Georges Lemaître 4, 1348 Louvain-la-Neuve, Belgium.*

Abstract

It is mandatory for an ocean model to represent accurately the different kinds of waves since they play a critical role in ocean dynamics. Quantifying the dispersion or dissipation errors of a given numerical scheme and comparing numerical methods is not an easy task especially when using unstructured grids. In this paper we use a general method fully independent of the numerical scheme and of the grid to analyse dispersion and dissipation errors. In particular we apply this method to the study of the $P_1^{NC} - P_1$ finite element pair applied to the shallow water equations. The influence of the grid is observed by comparing the convergence rates of the dispersion errors on Poincaré, Kelvin and Rossby waves. We observe a significative reduction of the convergence rate on unstructured meshes compared to structured grids for the $P_1^{NC} - P_1$ pair, while this rate remains unchanged when using other approaches as the $P_1 - P_1$ pair without stabilization or the discontinuous Galerkin method.

Key words: Linear non-conforming finite element, Unstructured Meshes, Dispersion and dissipation errors, Shallow water equations, Geophysical Flows

1 Introduction

The shallow water equations exhibit three kinds of waves, namely the Poincaré, Kelvin and Rossby waves. Those waves play a crucial role in ocean dynamics. The Rossby waves are very slow waves generated by the variability of the Coriolis parameter and propagating only westward. Those waves are known to intensify the western boundary currents and are responsible for the transfer of huge amounts of heat and energy. The Kelvin waves are non dispersive waves generated by the tides and the winds. They propagate along the coasts and exhibit an exponential decay away from the coastlines. Kelvin waves carry large amounts of energy and play then a crucial role in mixing and dissipation processes [Cushman-Roisin , 1994, Pedlosky , 1979, Majda , 2003]. Minor errors in those waves dispersion relations may lead to large lack of accuracy in climate and weather predictions. It is thus mandatory for an

ocean model to propagate those waves in an accurate way.
Another difficulty lies in the coupling between the momentum and continuity equations, which raises several issues for any kind of numerical methods like finite differences, finite volumes or finite elements. Solving a mixed formulation as the shallow water equations may lead to the generation of spurious modes for certain sets of grids and bases and to lack of accuracy in the dispersion relations especially for the faster waves.

Many studies have been carried on since three decades to investigate the dispersion properties of many numerical schemes. In particular, dispersion relations on finite differences schemes have been studied for gravity waves [Arakawa and Lamb , 1977, Batteen and Han , 1981, Randall , 1994, Beckers and Deleersnijder, 1993] and for the Rossby waves [Dukowicz , 1995, Wajsowicz , 1986]. The most common technique often used with finite differences on regular grids consists in introducing Fourier modes in the discrete representation of the spatial operators. After some algebraic manipulation, one thus obtain the analytical expression of a numerical dispersion relation corresponding to this particular scheme, grid, and Fourier mode. More recently, dispersion for finite elements techniques were investigated [Atkinson et al., 2004, Walters and Carey , 1983]. In particular, Le Roux et. al investigated many finite element pairs for solving the two-dimensional shallow water equations on structured grids [Le Roux et al., 2007, Le Roux and Pouliot , 2008]. It has been shown that pairs as the $P_2 - P_2$, MINI, $P_1^{NC} - P_1$ or $P_1 iso P_2 - P_1$ present no spurious elevation modes [Le Roux , 2005, Le Roux et al., 2007, 2005]. Some have been disregarded because of poor dispersion error properties compared to the $P_1^{NC} - P_1$ pair [Le Roux , 2005, Hanert et al., 2004, 2005], which seems to be the best compromise. This pair is now used since a few years to represent shallow water oceanic flows [e.g. Lambrechts et al., 2005, Hanert et al., 2004, 2005, 2007, White et al., 2007]. However, the authors considered this analysis as *one step of the selection process* since other important factors as variable element sizes and unstructured grids should be considered in further investigations.

The present work is a part of the SLIM project which consists in building a new generation of ocean models based on the finite element method and unstructured grids. In this framework, we built a new method for analyzing the dispersion properties of numerical schemes on unstructured grids [Bernard et al., 2008]. The dispersion and dissipation properties of the discontinuous Galerkin (DG) method have been studied, showing superconvergence properties with the polynomial interpolation order and confirming the DG method as a good candidate for ocean modelling.
The comparison between numerical methods on unstructured grids is a quite difficult task and the conclusions may eventually lean towards one method or another, depending on the problem under study. This modal analysis provides a way to fairly compare the dispersion and dissipation errors introduced by different numerical schemes on unstructured grids, and brings thus other informations for the element selection process. In particular, this paper investigates the dispersion errors of the $P_1^{NC} - P_1$ and its convergence rate on both structured and unstructured grids.

The first section is a reminder of the shallow water equations and their finite element discretization, in particular for the $P_1^{NC} - P_1$ element pair. The next section briefly describes the modal analysis presented in [Bernard et al., 2008]. The analytical expressions of the shallow water waves and their approximate and exact dispersion relations are given in the appendix. In particular, the classical analytical dispersion relationships based on the WKB approximation [e.g. Wentzel, 1926] are not accurate enough to perform a convergence study. We then developed another approach to obtain reference dispersion relations by solving numerically a 1D Sturm-Liouville relation. The last section eventually presents the results of this modal analysis applied to the finite element pair $P_1^{NC} - P_1$ and compares the convergence rates to the unstabilized $P_1 - P_1$ pair convergence on both structured and unstructured grids.

2 Finite Element Method for the shallow water equations

We seek to determine the depth-averaged horizontal velocity $\mathbf{v}(\mathbf{x}, t)$ and depth of the fluid layer $H(\mathbf{x}, t)$, both solutions of the following inviscid shallow water formulation:

$$\frac{\partial H\mathbf{v}}{\partial t} + \nabla \cdot (H\mathbf{v}\mathbf{v}) + f\mathbf{e}_z \times H\mathbf{v} = -gH\nabla\eta \tag{1}$$

$$\frac{\partial H}{\partial t} + \nabla \cdot (H\mathbf{v}) = 0 \tag{2}$$

where t is time, f is the Coriolis parameter, g is the gravitational acceleration and $\eta(\mathbf{x}, t)$ denotes the relative surface elevation of the fluid corresponding to the relation $H = H_0 + \eta$ with H_0 the reference depth of the fluid. The vector $\mathbf{e}_z$ denotes the local normal unit vector to the geopotential surface.
This set of equations represents the flow of a thin layer of incompressible fluid under the influence of a gravitational force in a rotating framework. Those equations can be obtained from the vertical integration of the incompressible 3D Navier-Stokes equations with impermeability boundary conditions on the surface and bottom of the ocean [Pedlosky , 1979, Cushman-Roisin , 1994]. The viscous terms of the Navier-Stokes equations are neglected. However, a subgrid scale viscosity could be added to take into account the influence of the subgrid scale processes.
In this work we neglect the non linear transport terms and the reference depth H_0 is assumed constant. The linearized shallow water equations (1) and (2) read:

$$\frac{\partial u}{\partial t} + g\frac{\partial \eta}{\partial x} - fv = 0, \tag{3}$$

$$\frac{\partial v}{\partial t} + g\frac{\partial \eta}{\partial y} + fu = 0, \tag{4}$$

$$\frac{\partial \eta}{\partial t} + H_0\left(\frac{\partial u}{\partial x} + \frac{\partial v}{\partial y}\right) = 0. \tag{5}$$

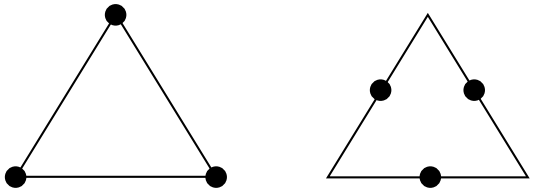

Fig. 1. P_1 linear conforming element (left) representing the water elevation and the P_1^{NC} linear non-conforming element (right) representing the velocity field.

A weak formulation may be obtained by multiplying the momentum and continuity equations by test functions $\widehat{\mathbf{v}} = (\widehat{u}, \widehat{v})$ and $\widehat{\eta}$ respectively, by integrating on the domain Ω and taking advantage of the divergence theorem for the continuity equation. More informations on the standard Galerkin procedure may be found in [Ciarlet , 1978, Hughes , 2000]. A possible weak formulation is:
Find $\mathbf{u} = (u, v)$ and η such that:

$$\begin{aligned} \int_\Omega \left(\frac{\partial u}{\partial t} + g\frac{\partial \eta}{\partial x} - fv \right) \widehat{u}\, d\Omega = 0, \\ \int_\Omega \left(\frac{\partial v}{\partial t} + g\frac{\partial \eta}{\partial y} + fu \right) \widehat{v}\, d\Omega = 0, \\ \int_\Omega \frac{\partial \eta}{\partial t}\widehat{\eta}\, d\Omega - \int_\Omega H_0 \left(u\frac{\partial \widehat{\eta}}{\partial x} + v\frac{\partial \widehat{\eta}}{\partial y} \right) d\Omega + \int_{\partial\Omega} H_0 u_n \widehat{\eta}\, dS = 0, \end{aligned} \tag{6}$$

where u_n denotes the normal velocity across the edge $\partial\Omega$. Setting this integration on boundaries to zero allows to weakly impose the impermeability conditions on the solid walls [e.g. Hanert et al., 2006]. Moreover, such a weak formulation allows us to consider non-continuous velocity fields.

We consider the use of the $P_1^{NC} - P_1$ pair depicted in Figure (1). The pressure, i.e. the water elevation, is represented as a continuous piecewise linear field and the velocity is a discontinuous piecewise linear field except at the mid-edges. The $P_1^{NC} - P_1$ element pair has been used for the first time to build a noise-free finite element two-layer shallow water model [Hua and Thomasset , 1984]. This pair became popular because it clearly exhibits the better numerical properties in terms of dispersion error and computational cost among the set of element pairs which do not suffer from elevation modes (i.e. the $P_2 - P_2$, MINI, $P_1^{NC} - P_1$ or $P_1 iso P_2 - P_1$ pairs) [Le Roux et al., 2007, Le Roux and Pouliot , 2008]. Indeed, the orthogonality of the non-conforming shape functions permits to reduce the computational costs. The discontinuities in the non-conforming elements represent a compromise between discontinuous and continuous fields and make the $P_1^{NC} - P_1$ a better suited element than continuous ones to represent advection dominated processes. Notice that some element pairs do not suffer from spurious elevation modes only in some particular cases, as the classical

$P_1 - P_1$ with the use of weakly imposed no normal flow boundary conditions on smooth domains [Hanert et al., 2006].

We then proceed to the spatial discretization of the unknown fields. The computational domain Ω is divided into a set of N non overlapping elements Ω_e with a total of N_e edges and N_v vertices, leading to $N_d = N_v + 2N_e$ degrees of freedom. We discretize the elevation and velocity fields by assuming a linear combination of nodal values and linear shape functions on each element:

$$u = \sum_{n=1}^{3} U_n \psi_n, \quad v = \sum_{n=1}^{3} V_n \psi_n, \quad \eta = \sum_{n=1}^{3} H_n \phi_n,$$

with (U_n, V_n) and H_n the nodal values and ψ_n and ϕ_n the shape functions for the velocity and elevation fields respectively.

Introducing this discretization into the weak formulation (6) with the weak imposition of the no normal flow boundary conditions , we obtain the following finite element system:

$$\mathbf{M}\frac{\partial \mathbf{U}}{\partial t} + \mathbf{A}\mathbf{U} = \mathbf{0} \tag{7}$$

where $\mathbf{U}$ is the vector of nodal values

$$\mathbf{U} = [U_j \; V_j \; H_l]^T ,$$

$\mathbf{M}$ is the global $N_d \times N_d$ mass matrix and $\mathbf{A}$ contains the gradient, divergence and Coriolis discrete operators:

$$\mathbf{A} = \left[\begin{array}{c|c|c} 0 & -\int_\Omega f\psi_i\psi_j \, d\Omega & \int_\Omega g\psi_i \frac{\partial \phi_l}{\partial x} \, d\Omega \\ \hline \int_\Omega f\psi_i\psi_j \, d\Omega & 0 & \int_\Omega g\psi_i \frac{\partial \phi_l}{\partial y} \, d\Omega \\ \hline -\int_\Omega H_0 \frac{\partial \phi_k}{\partial x}\psi_j \, d\Omega & -\int_\Omega H_0 \frac{\partial \phi_k}{\partial y}\psi_j \, d\Omega & 0 \end{array}\right] \tag{8}$$

with the subscripts $i, j = 1 \ldots N_e$ and $k, l = 1 \ldots N_v$.

The specific pattern of this matrix $\mathbf{A}$ allows the appearance of both velocity and elevation modes. Steady spurious modes are solutions of the system which are not physically relevant. They do not propagate in time, but are trapped into the mesh and are thus solution of the steady state formulation:

$$\mathbf{A}\mathbf{U} = \mathbf{0} \, . \tag{9}$$

Notice that specific spurious modes may also appear in some time-dependant problems, but those will not be considered in this paper. An analysis of such modes may be found in [Platzman , 1981].

To each eigenvector of the matrix $\mathbf{A}$ corresponds an elevation mode and a velocity mode.
A spurious pressure (or elevation) mode can be defined as a mode corresponding to a stationary eigenmode of the discrete system which has zero velocity components and a non constant pressure belonging to the kernel of the discrete gradient operator. A spurious velocity mode can be defined as a mode corresponding to a zero elevation with the velocity components belonging to the intersection of the kernel of the divergence operator and the kernel of the Coriolis operators. Such spurious modes have been found for the C grid and the RT_0-P_0, RT_0-P_1, BDM_1-P_0 and BDM_1-P_1 finite element schemes [Rostand et al, 2007]. Notice that RT_0 denotes here the velocity discretization used in the Raviart-Thomas finite element approximation, while P_0 or P_1 denotes the elevation discretization.

3 Discrete modal analysis of the shallow water waves

This section describes the modal analysis using the framework presented in [Bernard et al., 2008]. The main advantage of this alternative approach lies in the fact that it is based on the analysis of the discrete representation of the spatial operators, and it remains valid for any kind of numerical scheme or grid. This approach applied to structured grids will reproduce exactly the same numerical dispersion relations than the classic dispersion analysis obtained by other methods as for instance [Le Roux et al., 2007, Le Roux and Pouliot , 2008], but the approach remains valid on unstructured grids. Obviously, this numerical approach does not replace analytical approaches in the sense that it does not provide analytical expressions for the frequency, which can be used for instance to obtain analytical expressions of group and phase velocities. But it provides a way to analyse the impact of more realistic fully unstructured meshes on the dispersion relations, which contributes to the element selection process in the field of finite element ocean modelling.

In order to obtain a discrete dispersion relation, we first consider the semi-discrete formulation of the shallow water equations (7):

$$\frac{\partial \mathbf{U}}{\partial t} = \mathbf{L}\mathbf{U} \tag{10}$$

where $\mathbf{L} = \mathbf{M}^{-1}\mathbf{A}$ is the square matrix of the discrete space operators and $\mathbf{U}$ is the finite element discretization of the vector of unknowns.
We then assume the solution to be the real part of the following expression:

$$\mathbf{U}(x, y, t) = \mathbf{X}^h(x, y) \exp(i\omega t) \ . \tag{11}$$

with a general dependence in space $\mathbf{X}^h(x, y)$. Incorporating this expression (11) into the semi-discrete formulation (10) leads to the following eigenvalue problem:

$$[\mathbf{L} - \lambda \mathbf{I}]\mathbf{X}^h = \mathbf{0}. \tag{12}$$

For each eigenvalue λ_j ($j = 1 \dots N_d$), the corresponding discrete frequency ω_j and the associated numerical dissipation μ_j are found as the imaginary and real parts of the eigenvalue respectively:

$$\lambda_j = \mu_j + i\omega_j \quad .$$

We still need to compute the associated wave numbers in the x and y directions. This information is contained in the eigenvectors. To each eigenvector is associated an elevation mode $\eta_j(x, y)$ and a velocity mode $(u_j(x, y), v_j(x, y))$. We consider by instance the elevation mode and perform a 2D Fourier Transform to obtain the dominating wave number $\mathbf{k}_j = (k_{x,j}, k_{y,j})$ corresponding to this mode.
We obtain a discrete dispersion relation $\omega_j(\mathbf{k_j})$. A discrete dispersion analysis is then performed by comparing this relation to the reference dispersion relation $\omega(\mathbf{k_j})$. The absolute dissipation error of the mode j is computed as the absolute value of μ_j while the absolute dispersion error of mode j is given by:

$$\kappa_j = |\omega_j - \omega(\mathbf{k_j})| \quad .$$

It must be noticed that the Fourier transform only provides integer wave numbers. For the shallow water equations, those Fourier wave numbers are exact in the x direction, i.e. the longitudinal dimension, only if periodic boundary conditions are used, ensuring a sine dependence in x. But there is no guarantee to obtain such integer wave numbers in the y direction since the Coriolis parameter varies with the latitude and generates dispersive waves. With a non zero Coriolis force and dispersive waves, the y component of the wave number $\mathbf{k}$ has to be replaced by the reference exact wave number. The reference dispersion relations $\omega(\mathbf{k_j})$ for the dispersive shallow water waves have no analytical expression. They are computed numerically by solving a one-dimensional Sturm-Liouville relationship as described in the appendix.

4 Results

In this section we analyse the results from the modal analysis applied to the linearized shallow water equations with the β-plane assumption on the Coriolis parameter, $f = f_0 + \beta y$, using the $P_1^{NC} - P_1$ and the $P_1 - P_1$ finite element pairs on different structured and unstructured grids.
The reference solutions for comparison are provided by the Sturm-Liouville approach described in the appendix and the domain of computation is the semi-periodic square domain depicted in Figure (13). For all computations, the geometrical and physical parameters are $L = 10^6\ m$, $g = 10\ ms^{-2}$, $H_0 = 10^3\ m$, $\beta = 3\ 10^{-10}\ m^{-1}s^{-1}$ and $f_0 = 3\ 10^{-4}\ s^{-1}$. For those values, the typical non dimensional numbers are given by:

$$Ro = \frac{\sqrt{gH_0}}{Lf_0} = \frac{1}{3}, \qquad \frac{\beta L}{f_0} = 1$$

with Ro denoting the Rossby number. The shallow water equations are solved in a classi-

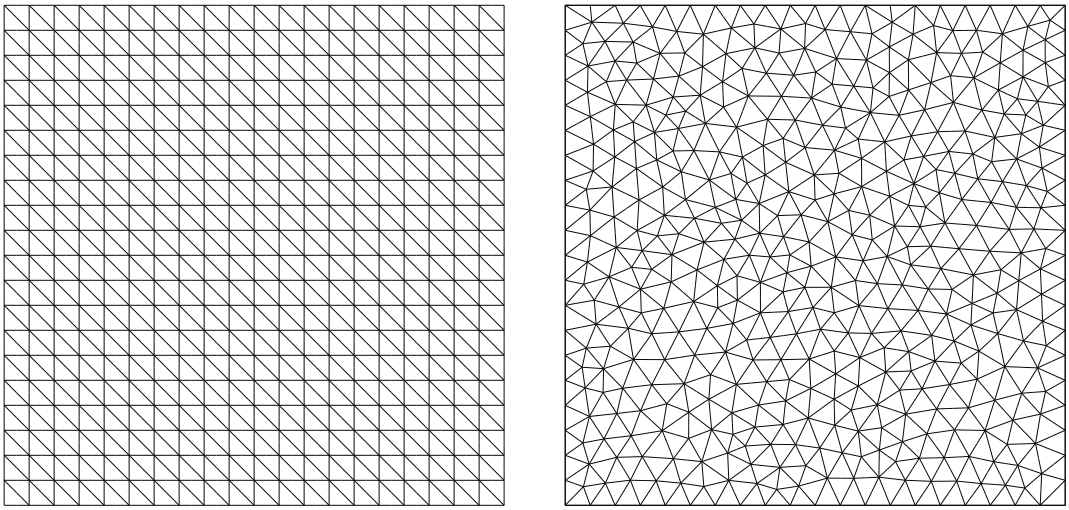

2921 degrees of freedom 3152 degrees of freedom

Fig. 2. Structured and unstructured meshes used for the computations on the semi-periodic domain with 800 and 866 elements respectively with the $P_1^{NC} - P_1$ finite element pair.

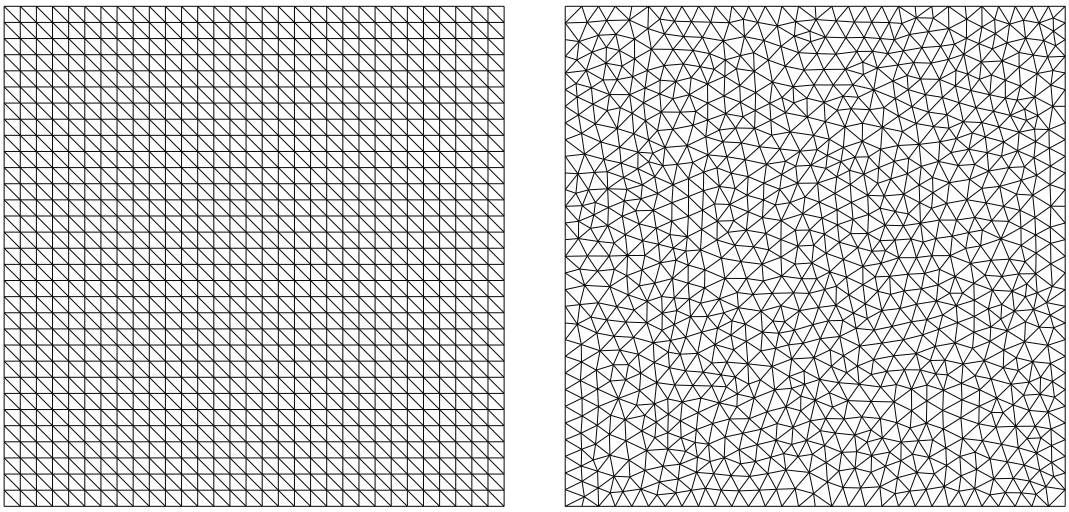

2700 degrees of freedom 2703 degrees of freedom

Fig. 3. Structured and unstructured meshes used for the computations on the semi-periodic domain with 1922 and 1920 elements respectively with the $P_1 - P_1$ finite element pair.

cal non dimensional version [Cushman-Roisin , 1994] in order to obtain a better numerical accuracy. This set of parameters presents an increased Coriolis parameter with an increased β-effect to visually differentiate the shape of Rossby modes in the y direction from sine functions. Indeed, a zero Coriolis parameter leads to gravity waves composed of sine and cosine modes, while a larger Coriolis parameter increases the dispersive nature of the Rossby and Poincaré waves. The only purpose of this arbitrary set of parameters is to visually identify

this dispersive behaviour and the difference with sine functions, as shown in Figure (7) or in table 1.
The structured and unstructured meshes used in our computations are depicted in Figure (2) and Figure (3) for the $P_1^{NC} - P_1$ and the $P_1 - P_1$ formulations respectively.

4.1 Dispersion errors for the $P_1^{NC} - P_1$ pair

The computation of the eigenvalue problem yields the set of eigenvalues depicted in Figure (4). As expected with the linear shallow water equations and the $P_1^{NC} - P_1$ pair, the scheme does not introduce any numerical dissipation, leading to fully imaginary eigenvalues. The reference dispersion curves and the numerical dispersion relations are presented in Figure (5) where we only considered the positive frequencies. The first modes corresponding to the dispersive Poincaré and Rossby waves are presented in Figure (6) and Figure (7) respectively, while Figure (8) exhibits the first modes of the Kelvin waves. We obtain as expected modes composed of sine functions in the x direction. The shapes of the Poincaré and Rossby modes in the y direction correspond to the modes obtained by the Sturm-Liouville 1D computation. The corresponding wave numbers are not integers as in sine functions, but are quite close to the corresponding sine wave numbers as shown in table 1. The Kelvin modes exhibit the expected exponential decay of equation (13) in the y-direction.

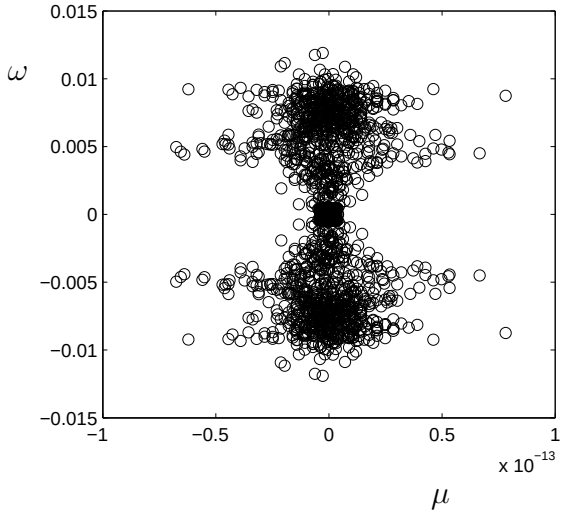

Fig. 4. Spectrum of eigenvalues λ corresponding to the $P_1^{NC} - P_1$ pair. The scheme does not introduce any dissipation to filter the unresolved modes, leading to fully imaginary eigenvalues with the dissipation $\mu = Im(\lambda)$ and the frequency $\omega = Re(\lambda)$.

Relative dispersion errors for the Poincaré, Rossby and Kelvin waves are shown in Figure (9) for the $P_1^{NC} - P_1$ pair (left column) and the $P_1 - P_1$ pair (right column). The convergence

j	1	2	3	4	5	6
$k_{y,j}$	3.1331	6.3411	9.4651	12.5966	15.7321	18.8696
$j\pi/L$	3.1416	6.2832	9.4248	12.5664	15.7080	18.8496

Table 1
Wavenumbers $k_{y,j}$ of the Sturm-Liouville problem (20) compared to their approximation $j\pi/L$.

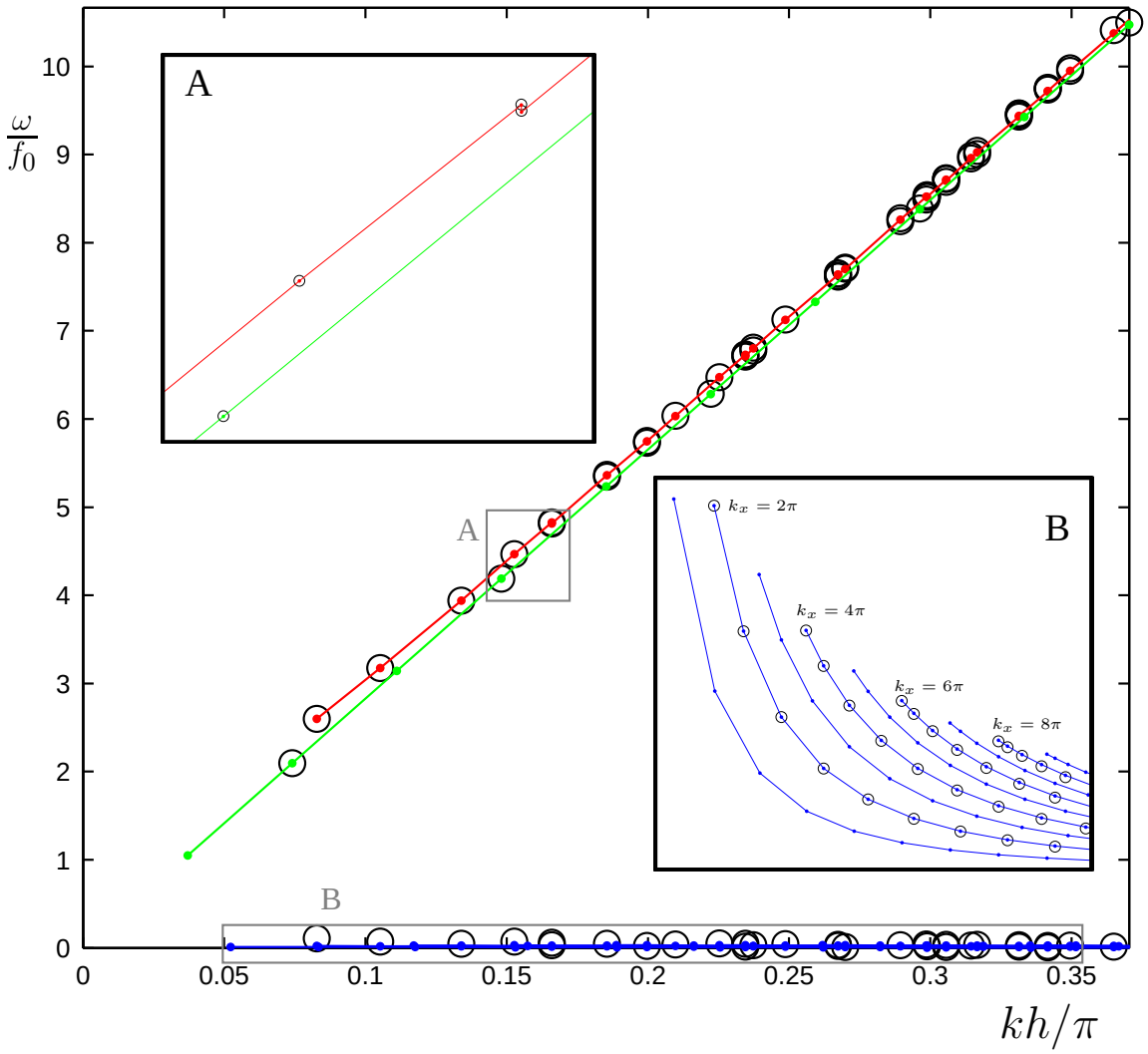

Fig. 5. Discrete dispersion relation of the Poincaré (red), Kelvin (green) and Rossby (blue) waves. The black circles correspond to the frequencies from the 2D finite element modal analysis while the dots from continuous lines are the reference frequencies from the 1D Sturm-Liouville approach. Poincaré and Kelvin modes are shown on the close up view A: the reference solution is made of different curves, so that two different couples (k_x, k_y) with two different frequencies may correspond to a same wave number. Rossby dispersion relations for different wave numbers k_x are depicted on close up view B, where only even k_x wave number are obtained because of periodic boundary conditions.

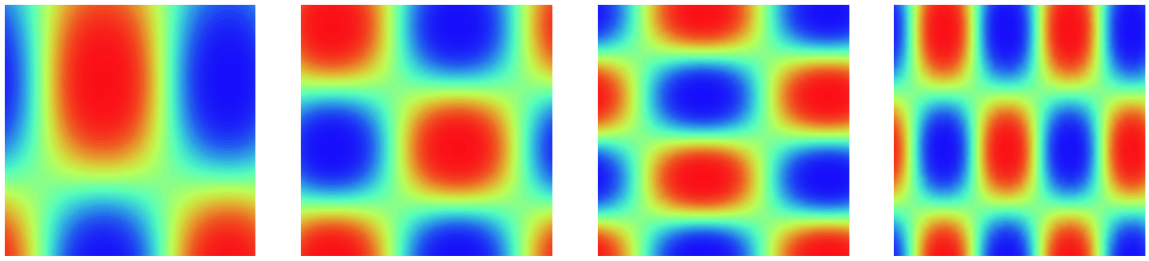

$k_x = 2, k_y = 1$ $k_x = 2, k_y = 2$ $k_x = 2, k_y = 3$ $k_x = 4, k_y = 4$

Fig. 6. Some of the Poincare first modes.

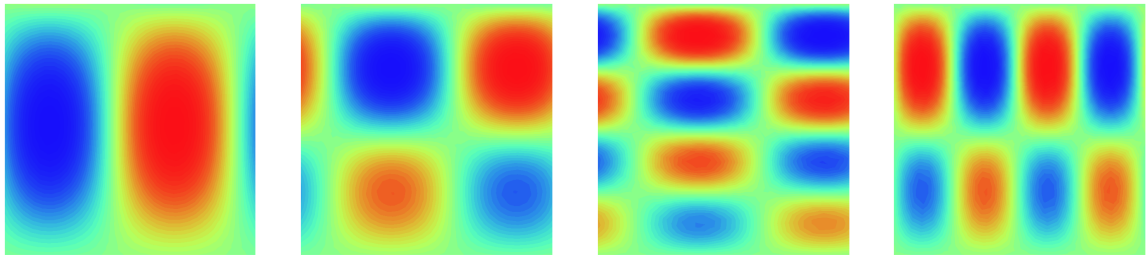

$k_x = 2, k_y = 1$ $k_x = 2, k_y = 2$ $k_x = 2, k_y = 4$ $k_x = 4, k_y = 4$

Fig. 7. Some of the Rossby first modes.

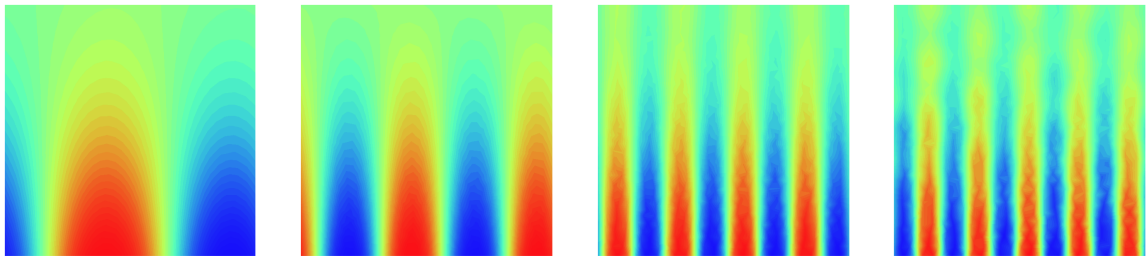

$k_x = 2$ $k_x = 4$ $k_x = 8$ $k_x = 10$

Fig. 8. Some of the Kelvin first modes.

rates are computed as the slope of the continuous lines, i.e. slopes of the linear approximations of the first resolved modes in the sense of the $\mathcal{L}_2$ norm. Since the error is proportional to the product of the element size h and the wave number k, $\mathcal{O}(kh)$, the convergence study is performed on only one grid, by considering the error variation with the wave number. Indeed, one way of computing the convergence of the dispersion errors is to consider several computations on different mesh with different element sizes h, and to compare the dispersion errors for one given mode. For sake of simplicity and in order to reduce the computational costs, we choose the second way which is to consider only one mesh and to compare the different resolved modes, which means considering a variation of k instead of a variation of h. Of course, this second approach is totally valid and equivalent to the first one and the convergence will be observed only if we consider the resolved modes far from the grid cutoff and if the shapes of the modes under study are close to sine functions, which is the case in this

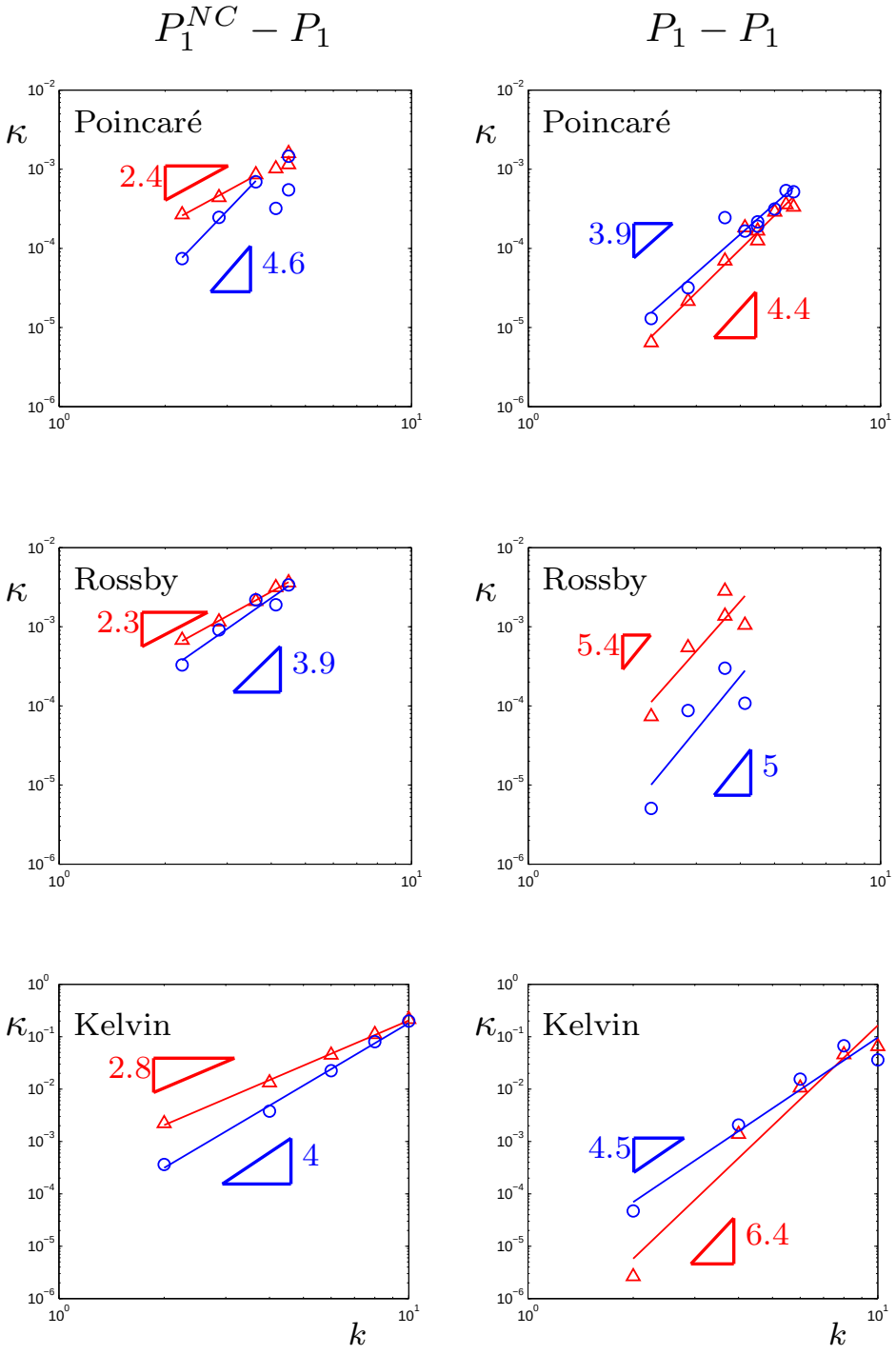

Fig. 9. Convergence of the relative dispersion error for the first resolved modes corresponding to the dispersive Poincaré (upper row), Rossby and Kelvin(lower row) waves on structured (blue circles) and unstructured (red triangles) meshes with the $P_1^{NC} - P_1$ pair (left) and the $P_1 - P_1$ pair (right). The use of structured meshes strongly decreases the convergence rates for the $P_1^{NC} - P_1$ pair while the rates remain unchanged for the $P_1 - P_1$ pair.

study, considering the physical parameters, the domain shape and boundary conditions used.

It has been shown that the Discontinuous Galerkin method exhibits superconvergence properties for the dissipation and dispersion errors [e.g. Hu and Atkins, 2002]. For polynomial shape functions of order p, the DG method provides a convergence rates of $2p+2$ for the relative dispersion errors and $2p+1$ for the relative dissipation errors if an even order is used. Same rates are reached for odd orders only if a Riemann solver is used in the flux computation instead of a center scheme. Those results have also been demonstrated [e.g. Ainsworth, 2004] for a 1D scalar transport equation. The same rates were obtained for the DG method with the same modal analysis for both structured and unstructured grids, for the Poincaré, Kelvin and Rossby waves [e.g. Bernard et al., 2008].
A fair comparison between a high order discontinuous method and other finite element pairs as the non-conforming $P_1^{NC} - P_1$ pair is not a simple task since the results depend in a large part on the problem under study, and in particular on the geometry and topology of the problem. A first comparison based on the dispersion errors criterion is provided by the modal analysis exposed in this paper, since both formulations are compared with the same method and the same number of degrees of freedom.

We observe in Figure (9) the difference between the $P_1^{NC} - P_1$ pair on structured grids (blue lines) and the same pair on unstructured grids (red lines). A first polynomial order DG method provides a convergence rate of 4 with a Riemann solver and of 2 with a centered scheme for the relative dispersion error. We observe here that the $P_1^{NC} - P_1$ pair exhibits a convergence rate as high as the P_1 DG method for structured grids, but the use of unstructured grids considerably reduces the rate, reaching about 2.5, which is similar to the rate of convergence of a finite volume method.

4.2 Comparison with the $P_1 - P_1$ pair

The same computation is performed on both kinds of grids with the $P_1 - P_1$ pair. We consider here a transient computation and the no normal flow boundary conditions are weakly imposed to avoid any spurious elevation mode with this pair. Moreover, solving the linear shallow water equations with this pair do not require the use of SUPG formulation to stabilize the scheme. The $P_1 - P_1$ pair is thus well suited for this particular simple computation, even though its is usually not recommended for solving mixed formulations.
Under those assumptions, we observe in the right column of Figure (9) the relative dispersion errors. The $P_1 - P_1$ pair exhibits the same rate of convergence of 4. For this modal analysis, such an element pair appears to be a better discrete space, as the formulation (12) is no more a constrained problem and the issue of spurious modes is no more relevant. For pure wave propagation, the use of the same discretization then appears to be a better choice in term of accuracy. It is still not quite clear why the $P_1^{NC} - P_1$ accuracy is strongly affected

and why the convegrence rate of the $P_1 - P_1$ pair remains unchanged when considering unstructured grids.

4.3 Influence of mesh perturbation with the $P_1^{NC} - P_1$ pair

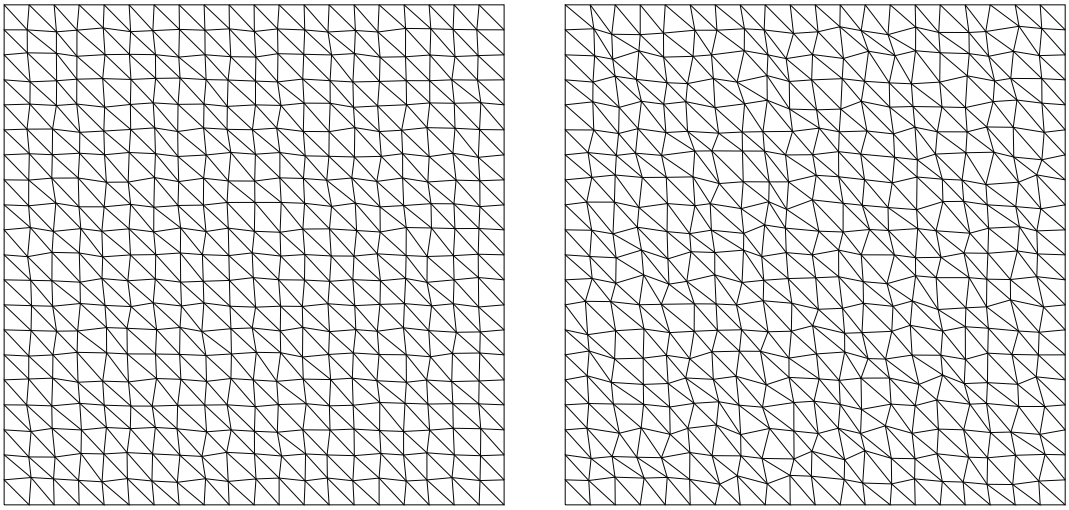

Fig. 10. Structured-distorded meshes used for the computations on the semi-periodic domain with 2921 degrees of freedom and 800 elements with the $P_1^{NC} - P_1$ finite element pair. The perturbation on the nodes coordinates is a random function presenting a maximum value of 10% of the element size h on the less distorded mesh (left) and of 20% on the more distorded mesh (right).

Given the strong degradation of the convergence rate of the $P_1^{NC} - P_1$ pair on unstructured grids, one might be interested in computing the convergence rates on slightly distorded structured grids. We consider the perturbed meshes depicted in Figure (10) and apply the same analysis. The convergences are depicted in Figure (11) for both structured-distorded meshes. We observe a fast degradation of the convergence rate when perturbing the structured nature of the mesh: the first slightly distorded mesh leads to a convergence rate of about 3.5 instead of 4 on the original structured mesh. The second larger perturbation leads to a rate of about 2.7, which is almost as low as the convergence rate on fully unstructured meshes.

4.4 Influence of the subgrid scale viscosity on the $P_1^{NC} - P_1$ pair

Finally, we observe that the higher order of convergence can be recovered on unstructured grids with the $P_1^{NC} - P_1$ pair by introducing a sufficient amount of subgrid scale viscosity scaling as $\mathcal{O}(h^2)$. The convergence for the Poincaré, Kelvin and Rossby waves are depicted in Figure (12). For a small viscosity of $\nu = 0.02h^2$ (red lines), the convergence rates are not much improved compared to the inviscid computation, while the use of a larger viscosity

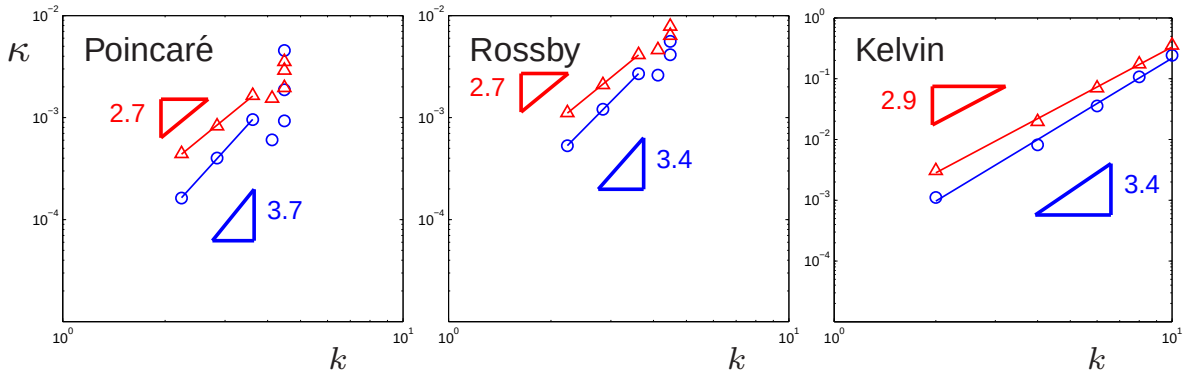

Fig. 11. Convergence of the relative dispersion error for the first resolved modes corresponding to the Poincaré (left), Rossby and Kelvin (right) waves on the less distorded structured mesh (blue circles) and the more distorded structured mesh (red triangles) with the $P_1^{NC} - P_1$ pair. The first slight perturbation of the mesh leads to a convergence rate of about 3.5 instead of 4, while the second perturbation leads to a rate equivalent to the rate on fully unstructured meshes.

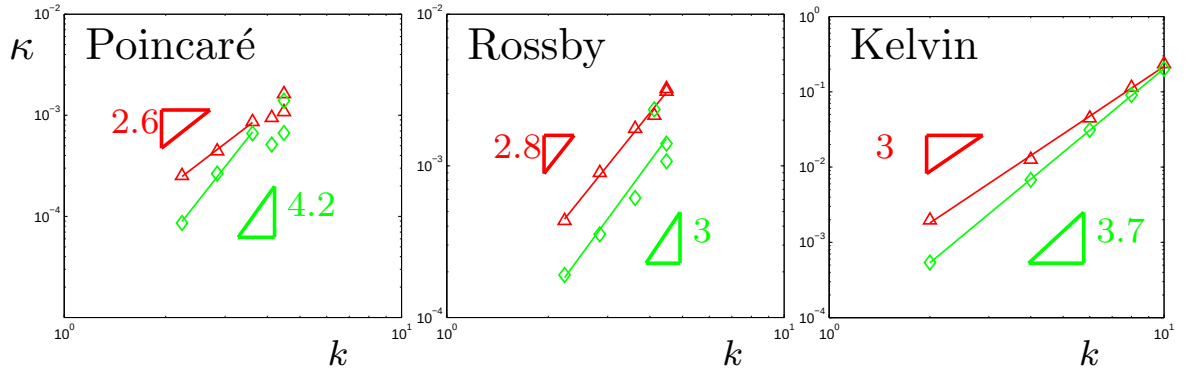

Fig. 12. Convergence of the relative dispersion error with subgridscale viscosities of $\nu = 0.02h^2$ (red triangles) and $\nu = 0.2h^2$ (green diamonds) for the first resolved modes corresponding to the Poincaré, Rossby and Kelvin waves on unstructured meshes with the $P_1^{NC} - P_1$ pair. The convergence rate on unstructured meshes is highly improved with the use of a sufficiently large subgrid scale viscosity.

$\nu = 0.2h^2$ (green lines) leads to recovering approximately the convergence of 4.

5 Conclusions

We have analyzed in this paper the dispersion properties of the $P_1^{NC} - P_1$ finite element pair by means of a general method, fully independent of the grid and of the numerical scheme. We obtained different convergence properties on structured and unstructured grids. The $P_1^{NC} - P_1$ pair leads to a convergence rate of the relative dispersion errors of 4 on structured grids, which is equivalent to the superconvergence properties of the piecewise linear DG method with the use of a Riemann solver, i.e. $2p+2$. This convergence of the $P_1^{NC} - P_1$

pair is *highly reduced on unstructured grids* and reach about 2.5 while the convergence rates of schemes as the DG method or the $P_1 - P_1$ pair remain unchanged on both kinds of grids. The convergence rate may however be recovered on unstructured meshes by introducing a sufficient amount of viscosity scaling as $\nu \propto \mathcal{O}(h^2)$ where h is the element size. However, the dissipation errors generated to recover the dispersion convergence rate often exceed the dispersion errors itself. Though certainly unacceptable for solving the wave equation, this option is however valid for an ocean model if the diffusivity associated to the subgrid scale processes exceeds the viscosity needed to recover the dispersion convergence rate.
Solving the mixed problem with the $P_1^{NC} - P_1$ pair avoids the issue of the spurious elevation modes generation. Moreover, the velocity discontinuities are quite usefull for introducing upwinding schemes when computing non-linear advection terms. But the $P_1^{NC} - P_1$ pair exhibits a *high sensitivity to the mesh structure and leads to a significative loss of convergence for the dispersion error on unstructured meshes* or even slightly distorded structured meshes.

Considering structured grids, it is well known that the convergence rate of the dispersion errors for inertia-gravity waves is $\mathcal{O}(h^4)$ for the $P_1^{NC} - P_1$ and $P_1 - P_1$ pairs, and only $\mathcal{O}(h^2)$ for pairs as $P_1 - P_1$, $P_1^{NC} - P_0$ or $P_1 iso P_2 - P_1$ [Le Roux et al., 2007]. In this paper, we restricted ourselves to the element pairs providing an $\mathcal{O}(h^4)$ convergence rate. One could argue that the reduced convergence of the $P_1^{NC} - P_1$ pair is not surprising and is due to the loss of symmetry in the discrete operators computation. Then, it would be more surprising that the convergence rate of the $P_1 - P_1$ pair remains unchanged on any kind of grid.
Anyway, even though numerical scheme comparison is a complex matter and cannot be reduced to a single criterion as the convergence properties of dispersion errors, this lack of accuracy of the $P_1^{NC} - P_1$ formulation on unstructured meshes is a real issue, especially in the framework of a finite element ocean model based on the use of unstructured grids. The use of more accurate pairs or methods on unstructured meshes should then be investigated, as for instance the discontinuous Galerkin method which does not suffer from such convergence rate reduction.

This study eventually points out the fact that the conclusions from analysis of pairs based on structured grids may be irrelevant in terms of convergence errors for unstructured grids. The results obtained on structured meshes cannot always be directly extended to unstructured ones and such dispersion analysis should then be carried on on unstructured meshes.

Acknowledgements

Paul-Emile Bernard is supported by the *Fonds pour la formation à la Recherche dans l'Industrie et dans l'Agriculture* (FRIA, Belgium). The present study was carried out within the scope of the project "A second-generation model of the ocean system" funded by the *Communauté Française de Belgique*, as *Actions de Recherche Concertées*, under contract

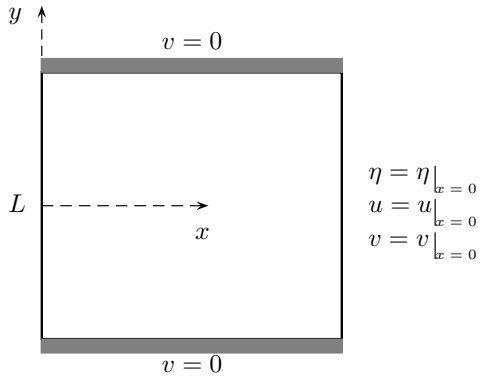

Fig. 13. Square domain of size L with solid walls on the northern and southern boundaries and periodic conditions on the eastern and western boundaries.

ARC 04/09-316. This work is a contribution to the SLIM [1] project.

Appendix

To analyse the ability of the finite element scheme to represent the dispersion and dissipation properties, we need to obtain a numerical dispersion relation: we solve the linear shallow water equations (3,4,5) on the semi-periodic domain depicted in Figure (13). The solid walls on the northern and southern boundaries allows the existence of Kelvin waves, while the semi-periodicity allows to assume sines eigenfunctions in the x direction and simplifies the analytical calculations:

$$\begin{aligned} \eta(0,y) &= \eta(L,y), \\ u(0,y) &= u(L,y), \\ v(0,y) &= v(L,y), \\ v(x,-L/2) &= 0 = v(x,L/2). \end{aligned}$$

We then search for analytical or at least reference dispersion relations to compare with.

The shallow water equations exhibits three families of waves: the Poincaré, Kelvin and Rossby waves. The Kelvin waves propagate only along the coasts and exhibit and exponential decay away from the coastlines. By assuming a coastline oriented along the east-west direction, we may derive the following expression of the Kelvin waves at midlatitudes

[1] SLIM, Second-Generation Louvain-la-Neuve Ice-ocean Model, *www.climate.be/SLIM*

[Majda , 2003]:

$$u(x,y,t) = \exp\left(-yf_0/\sqrt{gH_0}\right)\exp\left(i(k_x x - \omega t)\right) . \tag{13}$$

Kelvin waves are called non dispersive waves since the corresponding dispersion relation is linear, and thus independent of the Coriolis force:

$$\omega = \pm\sqrt{gH_0}k_x . \tag{14}$$

The Poincaré and Rossby waves are dispersive waves and analytical expressions of their dispersion relations requires many assumptions and simplifications.
We derive a third order wave equation in v by mixing the shallow water equations as proposed by Longuet-Higgins [Longuet-Higgins, 1965]:

$$\left(\frac{\partial}{\partial t}\left(-\frac{\partial^2}{\partial y^2} + \frac{1}{gH_0}\left(\frac{\partial^2}{\partial t^2} + f^2\right)\right) - \frac{\partial}{\partial x}\left(\beta + \frac{\partial}{\partial x}\frac{\partial}{\partial t}\right)\right)\frac{\partial v}{\partial t} = 0 . \tag{15}$$

The classical WKB approximation [e.g. Wentzel, 1926] leads to the following analytical dispersion relations for Poincaré and Rossby waves respectively:

$$\omega = \sqrt{f_0^2 + gH_0k^2} \tag{16}$$

$$\omega = \frac{gH_0\beta k_x}{f_0^2 + gH_0k^2} \quad . \tag{17}$$

$$\tag{18}$$

Those relations are very close to the exact dispersion relations and are widely used in the literature. But the lack of accuracy introduced by the WKB approximation is sufficient to prevent from convergence when compared to our numerical scheme. We then need to obtain the exact accurate dispersion relation to compare with.

Since we assume periodic boundary conditions on the eastern and western boundaries, we may assume sines functions in this x direction. The solution may be written as:

$$v(x,y,t) = Y(y)\exp\left(i(k_x x - \omega t)\right) \tag{19}$$

with the unknown function $Y(y)$ and the wave number in the x direction k_x.
As proposed in [Bernard et al., 2008], by substituting equation (19) in equation (15), the following typical Sturm-Liouville relation appears:

$$\frac{d^2Y}{dy^2} - \underbrace{\left[\frac{2f_0\beta}{gH_0}y + \frac{\beta^2}{gH_0}y^2\right]}_{g(y)}Y + \underbrace{\left[\frac{1}{gH_0}\left(\omega^2 - f_0^2\right) - \frac{\beta k_x}{\omega} - k_x^2\right]}_{k_y^2}Y = 0 . \tag{20}$$

This one-dimensional eigenvalue problem can be solved numerically with the appropriate solid walls boundary conditions $Y(-L/2) = 0 = Y(L/2)$. The eigenvectors are the modes $Y(y)$ in the y direction while the eigenvalues are k_y^2. We observe that for each couple (k_x, k_y), the corresponding frequencies are obtained by solving the third order equation:

$$\omega^3 - \left(gH_0k^2 + f_0^2\right)\omega - gH_0\beta k_x = 0 \tag{21}$$

with $k^2 = k_x^2 + k_y^2$. The two Poincaré frequencies propagating eastward and westward correspond to the larger roots in absolute value, while the smallest root corresponds to the Rossby frequency associated to this k_x, k_y couple. This method yields exact disperion relations with a variable Coriolis parameter for the Poincaré and Rossby waves.

References

M. Ainsworth. Dispersive and dissipative behavior of high order Discontinuous Galerkin finite element methods. *Journal of Computational Physics*, 198(1):106–130, 2004.

A. Arakawa, V.R. Lamb Computational design of the basic dynamical processes of the UCLA general circulation model *Methods Comput. Phys.*, 17:173–265, .

J.H. Atkinson, J.J. Westerink, R.A. Luettich Two dimensional dispersion analyses of finite element approximations to the shallow water equations *International Journal for Numerical Methods in Fluids*, 45:715–749, 2004.

M.L. Batteen, Y.-J. Han On the computational noise of finite-difference schemes used in ocean models *Tellus*, 33:387–396, 1981.

J.-M. Beckers and E. Deleersnijder. Stability of a fbtcs scheme applied to the propagation of shallow-water inertia-gravity waves on various space grids. *Journal of Computational Physics*, 108:95–104, 1993.

P.-E. Bernard, J.-F. Remacle, V. Legat and E. Deleersnijder. Dispersion analysis of Discontinuous Galerkin Schemes applied to Poincaré, Kelvin and Rossby waves *Journal of Scientific Computing*, 34:26–47, DOI:10.1007/s10915-007-9156-6, 2008.

P.G. Ciarlet *The Finite Element Method for Elliptic Problems* "Studies in Mathematics and its Applications" series, North-Holland, Amsterdam, 1978.

B. Cushman-Roisin *Introduction to Geophysical Fluid Dynamics* Prentice-Hall, 1994.

J.K. Dukowicz Mesh effects for Rossby waves *Journal of Computational Physics*, 119: 188–194, 1995.

B.L. Hua, F. Thomasset A noise-free finite element for the two-layer shallow water equations *Tellus*, 36 A:157–165, 1984.

E. Hanert, D.Y. Le Roux, V. Legat, and E. Deleersnijder. Advection schemes for unstructured grid ocean modelling. *Ocean Modelling*, 7:39–58, 2004.

E. Hanert. Towards a finite element ocean circulation model. *Ph.D. Thesis*, Université catholique de Louvain, 2004.

E. Hanert, D.Y. Le Roux, V. Legat, E. Deleersnijder An efficient Eulerian finite element method for the shallow water equations *Ocean Modelling*, 10:115–136, 2005.

E. Hanert and V. Legat. How to save a bad element with weak boundary conditions. *Computers and Fluids*, 35:477–484, 2006.

E. Hanert, E. Deleersnijder, S. Blaise and J.-F. Remacle. Capturing the bottom boundary layer in finite element ocean models. *Ocean Modelling*, 17:153–162, 2007.

F. Hu and H. Atkins. Eigensolution analysis of the Discontinuous Galerkin Method with Nonuniform Grids i One Space Dimension. *Journal of Computational Physics*, 182(2): 516–545, 2002.

T.J.R. Hughes *The Finite Element Method - Linear Static and Dynamic Finite Element Analysis* Dover, 2000.

J. Lambrechts, E. Hanert, E. Deleersnijder, P.-E. Bernard, V. Legat, J.-F. Remacle and E. Wolanski A high-resolution model of the whole Great Barrier Reef Hydrodynamics. *Estuarine, Coastal and Shelf Science* (submitted), 2007.

D. Le Roux, A. Sène, V. Rostand and E. Hanert. On some spurious mode issues in shallow-water models using a linear algebra approach. *Ocean Modelling*, 10:83–94, 2005.

D.Y. Le Roux, V. Rostand, B. Pouliot Analysis of numerically-induced oscillations in 2D finite-element shallow water models, Part I: Inertia-gravity waves *SIAM Journal on Scientific Computing*, 29:331–360, 2007.

D.Y. Le Roux Dispersion relation analysis of the P1NC-P1 finite element pair in shallow water models *SIAM Journal on Scientific Computing*, 27:394–414, 2005.

D.Y. Le Roux, B. Pouliot Analysis of numerically-induced oscillations in 2D finite-element shallow water models, Part II: Planetary waves *SIAM Journal on Scientific Computing* (in press), 2008.

M.S. Longuet-Higgins. Planetary waves on a rotating sphere, ii. *Proceedings of the Royal Society of London*, 284:40–68, 1965.

A. Majda. *Introduction to PDE's and waves for the atmosphere and ocean*. American Mathematical Society, 2003.

J. Pedlosky. *Geophysical Fluid Dynamics*. Springer-Verlag, Heidelberg, 1979.

G.W. Platzman Some Response Characteristics of Finite-Element Tidal Models *Journal of Computational Physics*, 40:36–63, 1981.

D.A. Randall Geostrophic Adjustment and the Finite-Difference Shallow-Water Equations *Monthly Weather Review*, 122:1371–1377, 1994.

V. Rostand, D.Y. Le Roux Raviart-Thomas and Brezzi-Douglas-Marini finite element approximations of the shallow water equations *International Journal for Numerical Methods in Fluids*, (published online), DOI:10.1002/fld.1668, 2007.

R.C. Wajsowicz Free Planetary Waves in Finite-Difference Numerical Models *Journal of Physical Oceanography*, 16:773–789, 1986.

R.A. Walters, G.F. Carey Analysis of spurious oscillation modes for the shallow water and Navier-Stokes equations *Computers and Fluids*, 11:51–68, 1983.

G. Wentzel. A generalization of quantum conditions for the purposes of wave mechanics. *Zeits. F. Phys.*, pages 38–518, 1926.

L. White and E. Deleersnijder. Diagnoses of vertical transport in a three-dimensional finite-element model of the tidal circulation around an island. *Estuarine Coastal and Shelf Science*, 74:655–669, 2007.